ACS OMEGA

Article

Cite This: ACS Omega 2019, 4, 5197−5203

http://pubs.acs.org/journal/acsodf

Heterobimetallic Single-Source Precursors: A Springboard to the Synthesis of Binary Intermetallics

Carena L. Daniels,[†] Deyny L. Mendivelso-Perez,[†,‡] Bryan A. Rosales,[†] Di You,[§] Sumit Sahu,[§,∥] J. Stuart Jones,[§,⊥] Emily A. Smith,[†,‡] François P. Gabbaï,[§] and Javier Vela*[,†,‡]

[†]Department of Chemistry, Iowa State University, Ames, Iowa 50011, United States

[‡]Ames Laboratory, Ames, Iowa 50011, United States

[§]Department of Chemistry, Texas A&M University, College Station, Texas 77843, United States

Supporting Information

ABSTRACT: Intermetallics are atomically ordered crystalline compounds containing two or more main group and transition metals. In addition to their rich crystal chemistry, intermetallics display unique properties of interest for a variety of applications, including superconductivity, hydrogen storage, and catalysis. Because of the presence of metals with a wide range of reduction potentials, the controlled synthesis of intermetallics can be difficult. Recently, soft chemical syntheses such as the modified polyol and ship-in-a-bottle methods have helped advance the preparation of these materials. However, phase-segregated products and complex multistep syntheses remain common. Here, we demonstrate the use of heterobimetallic single-source precursors for the synthesis of 10−15 and 11−15 binary intermetallics. The coordination environment of the precursor, as well as the exact temperature used play a critical role in determining the crystalline intermetallic phase that is produced, highlighting the potential versatility of this approach in the synthesis of a variety of compounds. Furthermore, we show that a recently developed novel plasma-processing technique is successful in removing the surface graphitic carbon observed in some of the prepared compounds. This new single-source precursor approach is a powerful addition to the synthesis of atomically ordered intermetallic compounds and will help facilitate their further study and development for future applications.

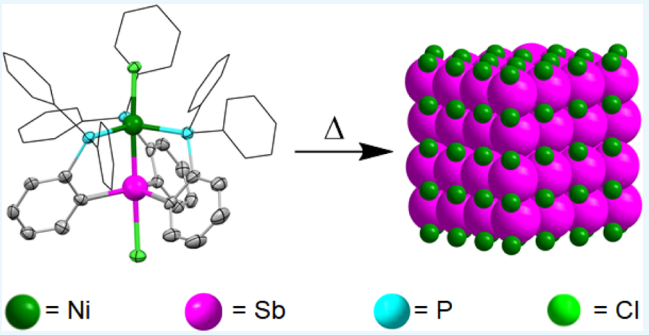

INTRODUCTION

Atomically ordered intermetallics are stoichiometric crystalline compounds in which main group and transition metals together adopt a unique structure that differs from that of its constituent elements. In addition to their rich and diverse structural chemistry, intermetallic compounds display important properties of interest for magnetism, superconductivity, catalysis, hydrogen storage, and shape-memory applications.[1−8] Often grown as single crystals, intermetallic compounds are typically made from the elements by traditional solid-state synthesis at relatively high temperatures—normally exceeding 1000 °C. As a result, it can be challenging to study their formation, measure their properties, or assess their practical utilization.

Recently, progress was made in the synthesis of intermetallic compounds by mild "soft" chemistry methods (Scheme 1).[9,10] One approach involves dissolving separate metal salts in tetraethylene glycol, which acts as a mild reducing agent under relatively modest temperatures.[11−19] This "modified polyol synthesis" method can be limited due to the different reduction potentials of the separate metal ions, leading in some cases to phase-segregated products rather than to the desired intermetallic compound. Very recently, a new templated approach was developed to overcome this problem.[20] Termed the "ship-in-a-bottle" method, it involves growing a porous oxide shell on a metal particle, followed by the addition of a second metal salt; the latter is able to permeate the porous shell and react with the original metal core, resulting in an encapsulated version of the intermetallic compound. Limitations include the multiple steps required to grow (and, if necessary, later remove) the porous oxide shell.

Single-source precursors—molecular complexes that contain all of the necessary elements required to make an inorganic material—were originally developed for the chemical vapor deposition of thin films.[21−25] Later, single-source precursors were successfully applied to the solution phase synthesis of colloidal nanomaterials.[25−29] Because of the presence of very different metals with dissimilar electronegativities and disparate reduction potentials, complex intermetallics are an ideal target for single-source precursors (SSPs). In this paper, we

Received: January 10, 2019
Accepted: February 25, 2019
Published: March 12, 2019

DOI: 10.1021/acsomega.9b00088
ACS Omega 2019, 4, 5197−5203

Scheme 1. Soft Synthesis of Intermetallic Compounds by (a) Modified Polyol Synthesis and (b) Ship-in-a-Bottle Methods; The Latter (b) Was Adapted with Permission from Maligal-Ganesh, R. V.; Xiao, C.; Goh, T. W.; Wang, L.-L.; Gustafson, J.; Pei, Y. Qi, Z.; Johnson, D. D.; Zhang, S.; Tao, F.; Huang, W. The Ship-in-a-Bottle Strategy To Synthesize Encapsulated Intermetallic Nanoparticle Catalysts: Exemplified for Furfural Hydrogenation. *ACS Catal.* 2016, *6*, 1754−1763; Copyright 2016 American Chemical Society[20]

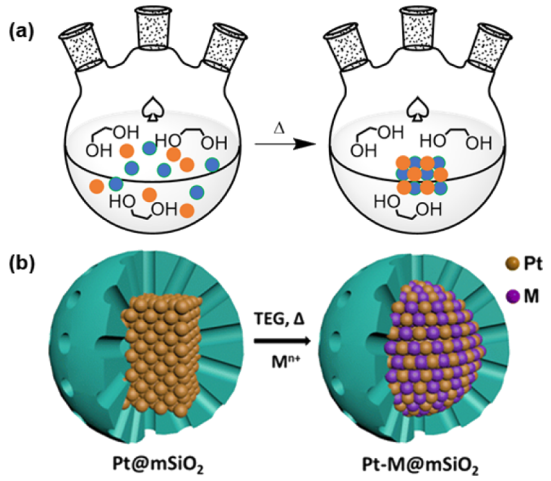

demonstrate the general synthetic utility of heterobimetallic single-source molecular precursors in the preparation of a wide range of binary 10−15 and 11−15 intermetallic compounds.

RESULTS AND DISCUSSION

Precursor Screening. A quick search in the Cambridge Structural Database[30] (CSD) is a great way to find well-characterized molecular compounds comprised of specific multiple elements (Scheme 2). Hits from the initial CCSD search can then be easily grouped into families of compounds supported by common or closely related ligands; they can also be narrowed down according to the desirable structural and bonding features, such as the presence of heterometal−metal interactions. A case in point is the family of heterobimetallic compounds shown in Scheme 3, all of which are supported by the same multidentate phosphine scaffold and contain a group 10 or 11 metal directly bonded to a group 15 element.[31−35] The presence of a common ligand platform allows for systematic synthetic variation by changing the identity of the metals or group substitution—of the R groups on the terminal phosphine or of the X ligands. In addition, the presence of a pre-existing, heterometal−metal bond bodes well for the use of these complexes as SSPs to the synthesis of atomically ordered intermetallics.

Establishing Scope and Tunability. Thermolysis of seven representative heterobimetallic complexes with varying transition-metal (Ni, Pd, Pt, or Au), pnictogen (As, Sb, or Bi), and ancillary ligand combinations demonstrates the utility of this platform in accessing several crystalline intermetallic compounds (Figure 1). Reflecting their original stoichiometry, thermolysis of several of the precursors produces "one-to-one" (1:1) binaries (NiAs, NiSb, PdSb, PtSb) that are known to adopt a common NiAs structure type (hexagonal, $P6_3/mmc$) (Table 1). In cases where the relevant phase diagram lacks any known one-to-one phases,[36] thermolysis produces other

Scheme 2. Flowchart for Screening Known Molecular Complexes as Potential SSPs

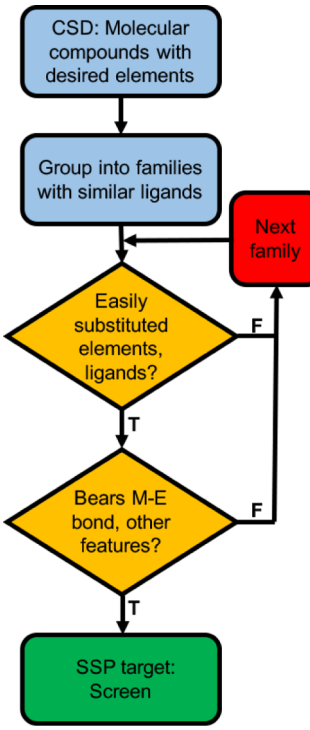

Scheme 3. (a) Di- and tri-(orthophosphino)heterobimetallic complexes; (b) SSP thermolysis

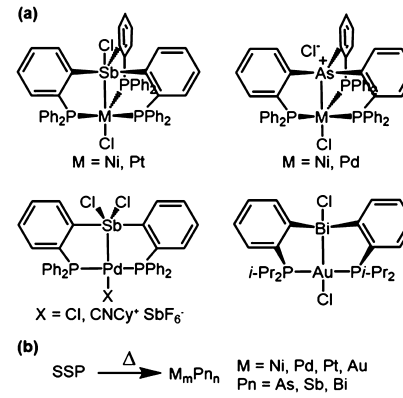

stoichiometries such as Pd_2As (hexagonal, $P\bar{6}2m$) and Au_2Bi (cubic, $Fd\bar{3}m$). Interestingly, thermolysis of the cationic precursor $[(CyNC)Pd(o\text{-}Ph_2P\text{-}C_6H_4)_2SbCl_2][SbF_6]$ produces PdSb, whereas thermolysis of the neutral analog $ClPd(o\text{-}Ph_2P\text{-}C_6H_4)_2SbCl_2$ produces $Pd_{20}Sb_7$ (trigonal, $R\bar{3}$, Figure 1d vs 1e, respectively). These divergent results strongly suggest that the specific ligand scaffold and metal coordination environment of the precursor precisely determine its mechanism and rate of decomposition, raising the prospect of fine tuning the outcome of thermolysis by group substitution or "molecular programming."[37−43]

Single Source versus Separate Precursors. Control experiments with separate commercially available precursors, thoroughly mixed and heated under the same conditions used to thermolyze the heterobimetallic complexes attest to the superiority of the latter. For example, $NiCl_2$ and Ph_3Sb fail to react with one another, whereas $Ni(COD)_2$ and Ph_3Sb do so

DOI: 10.1021/acsomega.9b00088
ACS Omega 2019, 4, 5197−5203

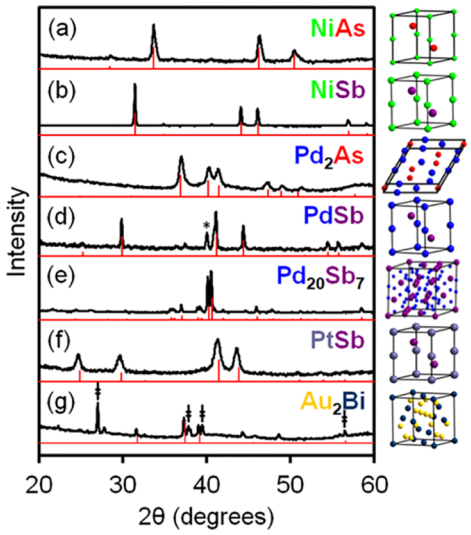

Figure 1. Powder XRD patterns of solids obtained after thermolysis of (a) [ClNi(*o*-Ph_2P-C_6H_4)$_3$As]Cl (600 °C), (b) ClNi(*o*-Ph_2P-C_6H_4)$_3$SbCl (600 °C), (c) [ClPd(*o*-Ph_2P-C_6H_4)$_3$As]Cl (475 °C), (d) [(CyNC)Pd(*o*-Ph_2P-C_6H_4)$_2$$SbCl_2$][$SbF_6$] (600 °C, * = Pd), (e) ClPd(*o*-Ph_2P-C_6H_4)$_2$$SbCl_2$ (450 °C), (f) ClPt(*o*-Ph_2P-C_6H_4)$_3$SbCl (340 °C), and (g) ClAu(*o*-iPr_2P-C_6H_4)$_2$BiCl (600 °C, ‡ = Bi). Standard patterns are shown in red.

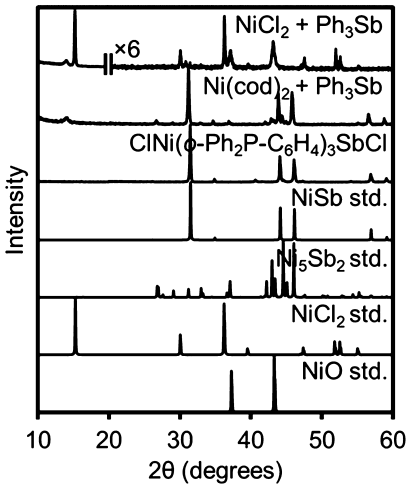

Figure 2. Powder XRD patterns of solids obtained after thermolysis of separate vs SSPs (600 °C).

uncontrollably, producing a mixture of NiSb and Ni_5Sb_2 (Figure 2). Therefore, thermolysis of ClNi(*o*-Ph_2P-C_6H_4)$_3$SbCl and other SSPs is a more reliable and generalizable approach to the preparation of binary intermetallics.

Precursor Decomposition and Phase Evolution. An added feature of the heterobimetallic SSPs presented here is their ability to produce different intermetallic compounds when heated to different temperatures. For example, thermolysis of ClPt(*o*-Ph_2P-C_6H_4)$_3$SbCl at 340, 450, or 600 °C produces phase-pure PtSb, a mixture of PtSb and Pt, or only Pt metal, respectively. Similarly, thermolysis of [ClPd(*o*-Ph_2P-C_6H_4)$_3$As]Cl at 475 or 600° C produces either phase-pure Pd_2As or a mixture of Pd_2As and $PdAs_2$, respectively. Finally, thermolysis of ClPd(*o*-Ph_2P-C_6H_4)$_2$$SbCl_2$ at 380, 450, or 600 °C produces phase-pure Pd_8Sb_3, phase-pure $Pd_{20}Sb_7$, or a mixture of PdSb and Pd_8Sb_3, respectively—see the Supporting Information.

Thermogravimetric analysis (TGA) and differential scanning calorimetry (DSC) coupled to online MS and IR analysis of evolved gases provide additional clues about the mechanism of thermal decomposition of SSPs (Figure 3). The two most common decomposition products are phenylchloride (PhCl) and triphenylphosphine (PPh_3) (Table 1 and Supporting Information). These are confirmed IR peaks corresponding to C(Ar)−H stretches slightly above 3000 cm^{-1} and C(Ar)−P stretches at 1100 and 1400 cm^{-1}. In the case of ClAu(*o*-iPr_2P-C_6H_4)$_2$BiCl, where R = iPr rather than phenyl (Scheme 3), MS and IR spectra are consistent with the evolution of di-isopropylphenylphosphine (iPr_2PPh) instead of Ph_3P. A majority of heterobimetallic complexes start to decompose between 270 and 340 °C, with the exception of [(CyNC)Pd(*o*-Ph_2P-C_6H_4)$_2$$SbCl_2$][$SbF_6$], which starts to decompose at only 173 °C. In this case, MS and IR show that this is accompanied by loss of cyclohexene (C_6H_{10}) from fragmentation of the cyclohexylisocyanide (CNCy) ligand. Therefore, a change in the nature of the monodentate ligand from phosphine to isocyanide can have a significant effect in lowering the temperature of thermolysis.

Interestingly, the difference between the total mass left after thermolysis, as measured by TGA, and the theoretical total

Table 1. Thermolysis of 10−15 and 11−15 Heterobimetallic SSPs

precursor	g/mol (%)	T_{dec}/°C[a]	XRD (°C)	g/mol (%)	Res. mass Δ[b]/%(°C)	gases[c]
[ClNi(*o*-Ph_2P-C_6H_4)$_3$As]Cl	988.37 (100)	340	NiAs (600)	133.62 (13.52)	43.29	PhCl, PPh_3
ClNi(*o*-Ph_2P-C_6H_4)$_3$SbCl	1035.20 (100)	315	NiSb (600)	180.45 (17.43)	28.17	PhCl, PPh_3
[ClPd(*o*-Ph_2P-C_6H_4)$_3$As]Cl	1036.10 (100)	300	Pd_2As (475)	287.76 (13.89)	40.98 (600)	PhCl, PPh_3
			Pd_2As + $PdAs_2$ (600)	(181.342)[e] (17.50)		
[(CyNC)Pd(*o*-Ph_2P-C_6H_4)$_2$$SbCl_2$][$SbF_6$]	1166.57 (100)	173	PdSb + Pd[d] (600)	228.18 (19.80)	21.53	C_6H_{10}
ClPd(*o*-Ph_2P-C_6H_4)$_2$$SbCl_2$	857.09 (100)	317	Pd_8Sb_3 (380)	1216.64 (17.74)	38.22 (600)	PhCl, PPh_3
			$Pd_{20}Sb_7$ (450)	2980.70 (17.39)		
			PdSb + Pd_8Sb_3 (600)	(1444.82)[f] (18.73)		
ClPt(*o*-Ph_2P-C_6H_4)$_3$SbCl	1171.59 (100)	270	PtSb (340)	316.84 (27.04)	42.43 (600)	Ph_2
			PtSb + Pt[d] (450)	316.84 (27.04)		
			Pt (600)	195.08 (16.65)		
ClAu(*o*-iPr_2P-C_6H_4)$_2$BiCl	863.35 (100)	319	Au_2Bi + Bi (600)	(811.89)[e] (47.02)	44.62	iPr_2PPh

[a]Thermal decomposition onset from TGA/DSC; multiple steps were observed in all cases. [b]Difference between % mass left after TGA and theoretical mass from inorganic binary alone (previous column): $\Delta = TGA^{f}_{m} - theo^{inor}_{m}$. [c]From IR−MS. [d]Minor impurity. [e]Average mass of hypothetical 1:1 binary (unknown). [f]Sum of masses of two binaries (1:1 + 8:3).

DOI: 10.1021/acsomega.9b00088
ACS Omega 2019, 4, 5197−5203

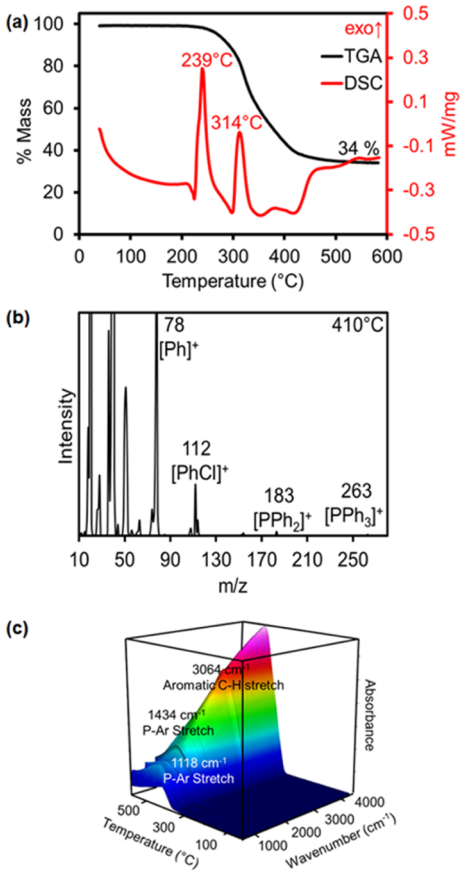

Figure 3. (a) TGA and DSC of ClNi(o-Ph_2P-C_6H_4)$_3$SbCl and (b) sample mass spectrum (410 °C) and (c) IR of gases evolved during its decomposition from 45 to 600 °C.

inorganic mass, calculated only from the content of group 10 or 11 transition-metal (M) and group 15 (Pn) elements, points to the presence of some leftover organics in a few of the intermetallic products (Table 1). Because only crystalline inorganic compounds are observed by X-ray diffraction (XRD), we conclude that these residues must be made of either an amorphous or semicrystalline material. Interestingly, despite thermolysis occurring in the absence of additional solvents or surfactants, transmission electron microscopy (TEM) shows that the intermetallic products are made of nanocrystalline particles (Figure 4 and Supporting Information).

Fate and Removal of Carbon. To probe the nature of the excess mass observed after thermolysis, we used Raman spectroscopy (Figure 5). A Raman peak observed at about 1340 cm^{-1} corresponds to disordered and structural defects within the graphitic sp^2 carbons (known as the D or A_{1g} band), whereas another at 1570 cm^{-1} corresponds to the doubly degenerate in-plane sp^2 C−C stretching mode (known as the G or E_{2g} band). A third Raman peak around 2680 cm^{-1}, indicative of layered graphene (a D-band overtone known as the 2D band) is absent from our samples. On the basis of this information, we conclude that the residual organics observed in some of the intermetallic compounds prepared here is mostly made of graphitic carbon.[44−46] Critically, there is a good correlation between the amount of excess mass measured by TGA and the relative intensity of the graphitic peaks, as observed by Raman spectroscopy (Figure 5a).

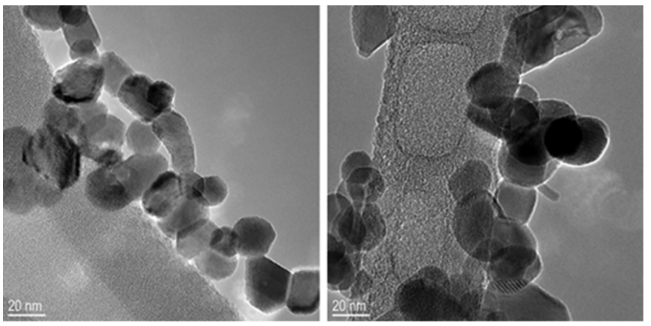

Figure 4. Representative TEM of 24 ± 6 nm PtSb produced by thermolysis of ClPt(o-Ph_2P-C_6H_4)$_3$SbCl at 340 °C. Observed lattice fringes with d-spacings of 2.02 and 2.99 Å correspond to (−120) and (011) lattice planes of PtSb.

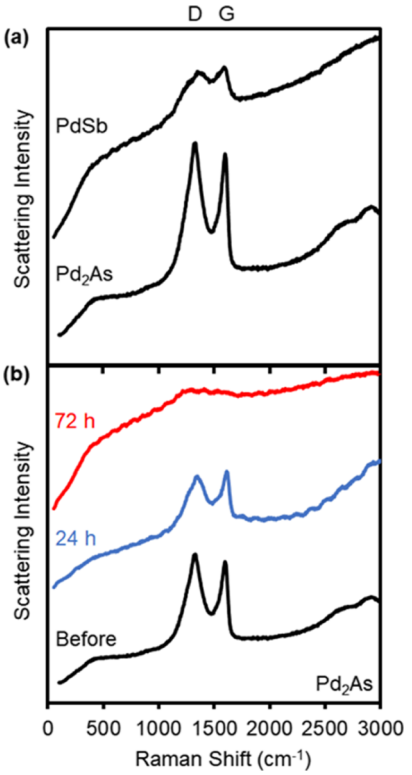

Figure 5. Raman spectra of intermetallic compounds (a) containing negligible (PdSb, 2%) vs noticeable (Pd_2As, 24%) residual mass upon thermolysis and (b) Pd_2As before and after cleaning under an O_2 plasma.

The presence of associated graphitic carbon could be advantageous in some applications such as catalysis or electrochemistry.[47,48] However, it can sometimes slow down the further development of materials for other applications. Therefore, we sought to remove this impurity from the surface of the intermetallic compounds. To do this, we employed plasma cleaning or "processing", which was recently shown to be superior to calcination in the removal of organic ligands and other carbonaceous materials from the surface of nanocrystal assemblies, without negatively impacting their structure. Typically, the gases employed are O_2 or He. Both have been shown to effectively remove carbon from the surface of various nanoparticles without detrimentally affecting their properties.[49−53] Using Pd_2As under an O_2 plasma as an example, we find that the graphitic peak intensities greatly decrease after 24

DOI: 10.1021/acsomega.9b00088
ACS Omega 2019, 4, 5197−5203

h and mostly disappear after 72 h of plasma processing (see Figure 5b and Experimental Section). To avoid the risk of oxidation, He plasma could be employed too, but carbon removal was slower in this case.

CONCLUSIONS

Atomically ordered intermetallics, often grown as single crystals at relatively high temperatures, were recently made by milder soft chemistry methods. However, phase segregation or multistep reactions remain common challenges. A search in the CCSD allowed us to identify a family of heterobimetallic complexes containing the desirable SSP features, such as the presence of a common and flexible ligand platform and the presence of a pre-existing heterometal−metal bond.

Thermolysis of these heterobimetallic precursors consistently produces crystalline binary phases containing both metals, confirming our hypothesis that these complexes are ideal single-source precursors to atomically ordered intermetallics. Control studies demonstrate that SSPs are superior to separate precursors in producing the desired intermetallic products under otherwise identical reaction conditions. The specific ligand coordination environment affects the specific product phase, suggesting that the mechanism and rate of decomposition can be tuned by group substitution or "molecular programming." Additionally, heating the precursors to different temperatures also affects the specific product phase, providing more opportunities for tunability.

TGA−DSC coupled with evolved gas analysis by MS−IR are powerful tools to investigate the mechanism of thermal decomposition of heterobimetallic precursors. Through Raman analysis, we were able to determine that the excess mass leftover after thermolysis of some of these precursors is made of a thin layer of graphitic carbon on the intermetallic surface. Conveniently, this carbonaceous residue can be removed through plasma processing without negatively impacting the structure of the intermetallic compound. This new single-source precursor approach is a powerful addition to the synthesis of binary intermetallics and will help speed up their study and development for future applications.

EXPERIMENTAL SECTION

Materials. The heterobimetallic complexes, [ClNi(*o*-Ph_2P-$C_6H_4)_3As$]Cl,[31] $ClNi(o\text{-}Ph_2P\text{-}C_6H_4)_3SbCl$,[32] $ClAu(o\text{-}iPr_2P\text{-}C_6H_4)_2BiCl$,[33] $ClPt(o\text{-}Ph_2P\text{-}C_6H_4)_3SbCl$,[34] and $ClPd(o\text{-}Ph_2P\text{-}C_6H_4)_2SbCl_2$,[35] were prepared according to literature procedures. $[(CyNC)Pd(o\text{-}Ph_2P\text{-}C_6H_4)_2SbCl_2][SbF_6]$ and [ClPd(*o*-Ph_2P-$C_6H_4)_3As$]Cl are synthesized as follows. $NiCl_2$ (anhydrous, 98%), bis(1,5-cyclooctadiene)nickel (0) (Ni(COD)$_2$, 98+%), Ph_3Sb (97%), cyclohexyl isocyanide (CyNC, 98%), and $AgSbF_6$ (99%) were purchased from Strem and used as received. CH_2Cl_2, Et_2O, and tetrahydrofuran (THF) were purchased from Fisher Chemical, and celite was purchased from MilliporeSigma. CD_2Cl_2 and $CDCl_3$ were purchased from Cambridge Isotope Labs and used as received. CH_2Cl_2 was dried over alumina using a column-based solvent purification system from MBraun. Et_2O and THF were refluxed under N_2 over Na/K and distilled prior to use. All precursor syntheses were carried out in air.

Synthesis. *[(CyNC)Pd(o-Ph_2P-$C_6H_4)_2SbCl_2$][SbF_6].* (*o*-Ph_2P-$C_6H_4)_2SbCl$ (34 mg, 0.05 mmol) was mixed with $PdCl_2$(COD) (14 mg, 0.05 mmol) in CH_2Cl_2 (4 mL). After 2 h, cyclohexyl isocyanide (8 μL, 0.06 mmol) and $AgSbF_6$ (17 mg; 0.05 mmol) were sequentially added, and stirring continued for 16 h. The mixture was evacuated to dryness and the residue washed with Et_2O, taken up in CH_2Cl_2 (2 mL), and filtered through celite. Solvent evaporation afforded a yellow solid (33 mg, yield: 56%). Single crystals suitable for XRD were obtained by slow diffusion of Et_2O into a CH_2Cl_2 solution at ambient temperature (21 °C or RT). ^{1}H NMR (499.42 MHz; CD_2Cl_2): δ 8.33 (d, 2H, $^3J_{H-H}$ = 7.7 Hz), 7.95 (dd, 2H, $^3J_{H-H}$ = 10.7 Hz, $^3J_{H-H}$ = 4.3 Hz), 7.72 (dd, 2H, $^3J_{H-H}$ = 10.7 Hz, $^3J_{H-H}$ = 4.3 Hz), 7.66−7.54 (m, 22 H), 3.82 (s, 1H), and 1.59−1.16 (m, 10H). ^{13}C{^{1}H} NMR (125.58 MHz; CD_2Cl_2): δ 136.11 (s), 135.51 (s), 133.61 (t, J_{C-P} = 6.9 Hz), 133.30 (s), 132.37 (t, J_{C-P} = 3.3 Hz), 131.08 (br s), 130.32 (t, J_{C-P} = 5.7 Hz), 128.43 (s), 31.71 (s), 24.73 (s), and 22.41 (s). ^{31}P{^{1}H} NMR (121.49 MHz; CD_2Cl_2): δ 53.9.

[ClPd(o-Ph_2P-$C_6H_4)_3As$]Cl. A solution of $PdCl_2$(COD) (70 mg, 0.25 mmol) in CH_2Cl_2 (3 mL) was added dropwise to a stirred suspension of (*o*-Ph_2P-$C_6H_4)_3As$ (212 mg, 0.25 mmol) in CH_2Cl_2 (ca. 5 mL) Stirring for 12 h gave a red suspension. The mixture was filtered, washed with THF (2 mL), and dried in vacuo to afford a dark red powder (55 mg, yield: 78%). Single crystals suitable for XRD were obtained by slow diffusion of Et_2O into a chloroform solution at RT. ^{1}H NMR (499.42 MHz; $CDCl_3$): δ 8.33 (d, 3H, $^3J_{H-H}$ = 8.0 Hz), 8.17 (t, 3H, $^3J_{H-H}$ = 7.6 Hz), 7.65 (d, 3H, $^3J_{H-H}$ = 7.3 Hz), 7.42 (d, 3H, $^3J_{H-H}$ = 7.7 Hz), 7.22 (dd, 6H, $^3J_{H-H}$ = 8.0 Hz, $^3J_{H-H}$ = 7.2 Hz), 7.13−7.05 (m, 12H), and 7.02 (dd, 12H, $^3J_{H-H}$ = 7.5 Hz, $^3J_{H-H}$ = 7.3 Hz). ^{13}C{^{1}H} NMR (100 MHz; $CDCl_3$): δ 135.5 (s), 135.3 (s), 134.6 (br s), 132.9 (s), 132.4(s), 130.3 (s), and 128.8 (s). ^{31}P{^{1}H} NMR (202.16 MHz; $CDCl_3$): δ 39.9.

Thermolysis. *Single Source Precursors.* TGA and DSC were carried out on a Netzsch DSC/TGA (STA449 F1) coupled with a mass spectrometer and an infrared spectrophotometer for the analysis of evolved gases. The heterobimetallic precursor (5−20 mg) was placed in an alumina crucible, inserted into the TGA−DSC furnace, and placed under an inert Ar atmosphere. The temperature was increased from 45 to 600 °C at a rate of 10 °C/min. Mass spectra from 10 to 300 amu and FT-IR spectra of the evolved gases were measured at a rate of 10 scans per min. After cooling to RT, the remaining solids were removed and analyzed by powder XRD.

Separate Precursors.[54] Equimolar amounts (0.1 mmol each) of Ni ($NiCl_2$, 16 mg or Ni(COD)$_2$, 21 mg) and Ph_3Sb (35 mg) were ground together in a mortar with a pestle. The mixture was transferred to an alumina crucible, placed in a tube furnace, purged with N_2 gas for 30 min, and heated from 21 to 600 °C at a rate of 10 °C/min under continuous N_2 flow. After cooling to RT, the remaining solids were removed and analyzed by powder XRD.

Plasma Processing. Samples deposited on a glass slide were exposed to low temperature plasma using a Harrick's etcher (PDC-001) with PlasmaFlo gas mixer, O_2 as the feed gas, and 30 W power at 500 mTorr.[49−53]

Structural Characterization. *Single Crystal XRD.* Single crystal XRD measurements were performed at 110(2) K using a Bruker APEX-II CCD area detector diffractometer (Mo Kα radiation, λ = 0.71069 Å). In each case, a specimen of suitable size and quality was selected and mounted onto a nylon loop. The structures were solved by direct methods, which successfully located most of the nonhydrogen atoms. Semi-empirical absorption corrections were applied. Subsequent refinement on F^2 using the SHELXTL/PC package (v. 6.1) allowed location of the remaining nonhydrogen atoms.

DOI: 10.1021/acsomega.9b00088
ACS Omega 2019, 4, 5197−5203

Powder XRD. Powder XRD was collected using a Cu Kα radiation source on a Rigaku Ultima IV (40 kV, 44 mA) diffractometer. Each sample was prepared by drop-casting hexane suspensions onto a background-less quartz slide.

Spectroscopy. *NMR.* NMR spectroscopy was recorded at RT on a Varian Unity Inova 500 FT NMR (499.42 MHz for ^{1}H, 125.58 MHz for ^{13}C, 202.16 MHz for ^{31}P), Inova 400 FT NMR (100 MHz for ^{13}C), and an Inova 300 FT NMR (121.49 MHz for ^{31}P). ^{1}H and ^{13}C{^{1}H} NMR chemical shifts are given in ppm and referenced against $SiMe^{4}$ using residual solvent signals as secondary standards. ^{31}P{^{1}H} NMR chemical shifts are given in ppm and referenced against H_3PO_4 as an external standard.

Raman Spectroscopy. Raman spectroscopy analyses were performed using an XploRa Plus confocal Raman upright microscope, equipped with a Synapse EMCCD camera (Horiba Scientific/NJ, France). Diode lasers (532 and 785 nm) were used at 0.3 and 0.9 mW power, respectively. The 532 nm excitation laser was used for the analysis of PtSb, NiSb, Pd_2As, PdSb, and Au_2Bi samples, whereas the 785 nm excitation laser was used for the NiAs sample. A 50× air objective (Olympus, LMPlanFL) with a 0.5 numerical aperture was used to collect the Raman signal at five different locations on the sample with a 30 s acquisition time and 2 accumulations. Reported spectra were recorded with a 600 grooves/mm grating.

■ ASSOCIATED CONTENT

Supporting Information

The Supporting Information is available free of charge on the ACS Publications website at DOI: 10.1021/acsomega.9b00088.

Additional TGA, DSC, MS, IR, XRD, Raman, NMR, crystallographic, and TEM data, reaction scheme, visual appearance of the precursor, optical micrograph of the intermetallic product, TGA-DSC, IR, MS of evolved gases, Raman spectra of intermetallic compounds produced by thermolysis of heterobimetallic single source precursors, asymmetric unit of [(CyNC)Pd(*o*-Ph_2P-C_6H_4)$_2$$SbCl_2$][$SbF_6$], displacement ellipsoid plot of [ClPd(*o*-Ph_2P-C_6H_4)$_3$As]Cl, and selected bond lengths and angles (PDF)

Single crystal XRD data (CIF)

(PDF)

(CIF)

■ AUTHOR INFORMATION

Corresponding Author

*E-mail: vela@iastate.edu.

ORCID

Deyny L. Mendivelso-Perez: 0000-0001-8261-5081

Sumit Sahu: 0000-0001-7409-9275

Emily A. Smith: 0000-0001-7438-7808

François P. Gabbaï: 0000-0003-4788-2998

Javier Vela: 0000-0001-5124-6893

Present Addresses

$^{\parallel}$Current affiliation: Intel Corporation, 2501 NE Century Blvd., Hillsboro, OR 97124.

$^{\perp}$Current affiliation: Phillips 66 Research Center, Highway 60 Highway 123, Bartlesville, OK 74004.

Notes

The authors declare no competing financial interest.

■ ACKNOWLEDGMENTS

J.V. thanks the U.S. National Science Foundation for a CAREER grant from the Division of Chemistry, Macromolecular, Supramolecular and Nanochemistry program (1253058). F.P.G. thanks the U.S. National Science Foundation (CHE-1566474) and the Welch Foundation (A-1423). The authors thank Ludovico Cademartiri for assistance as well as Pat Thiel for comments.

■ REFERENCES

(1) Furukawa, S.; Komatsu, T. Intermetallic Compounds: Promising Inorganic Materials for Well-Structured and Electronically Modified Reaction Environments for Efficient Catalysis. *ACS Catal.* **2017**, *7*, 735−765.

(2) Gilroy, K. D.; Ruditskiy, A.; Peng, H.-C.; Qin, D.; Xia, Y. Bimetallic Nanocrystals: Syntheses, Properties, and Applications. *Chem. Rev.* **2016**, *116*, 10414−10472.

(3) Yan, Y.; Du, J. S.; Gilroy, K. D.; Yang, D.; Xia, Y.; Zhang, H. Intermetallic Nanocrystals: Syntheses and Catalytic Applications. *Adv. Mater.* **2017**, *29*, 1605997.

(4) Jana, S. Advances in Nanoscale Alloys and Intermetallics: Low Temperature Solution Chemistry Synthesis and Application in Catalysis. *Dalton Trans.* **2015**, *44*, 18692−18717.

(5) Lee, S.; Kim, H. J.; Lim, E. J.; Kim, Y.; Noh, Y.; Huber, G. W.; Kim, W. B. Highly Selective Transformation of Glycerol to Dihydroxyacetone Without Using Oxidants by a PtSb/C-Catalyzed Electrooxidation Process. *Green Chem.* **2016**, *18*, 2877−2887.

(6) Marakatti, V. S.; Peter, S. C. Nickel−Antimony Nanoparticles Confined in SBA-15 as Highly Efficient Catalysts for the Hydrogenation of Nitroarenes. *New J. Chem.* **2016**, *40*, 5448−5457.

(7) Shanbogh, P. P.; Peter, S. C. Low Cost Nano Materials Crystallize in the NiAs structure Type as an Alternative to the Noble Metals in the Hydrogenation Process. *RSC Adv.* **2013**, *3*, 22887−22890.

(8) Hou, H.; Cao, X.; Yang, Y.; Fang, L.; Pan, C.; Yang, X.; Song, W.; Ji, X. NiSb Alloy Hollow Nanospheres as Anode Materials for Rechargeable Lithium Ion Batteries. *Chem. Commun.* **2014**, *50*, 8201−8203.

(9) White, M. A.; Thompson, M. J.; Miller, G. J.; Vela, J. Got LiZnP? Solution Phase Synthesis of Filled Tetrahedral Semiconductors in the Nanoregime. *Chem. Commun.* **2016**, *52*, 3497−3499.

(10) White, M. A.; Miller, G. J.; Vela, J. Polytypism and Unique Site Preference in LiZnSb: A Superior Thermoelectric Reveals its True Colors. *J. Am. Chem. Soc.* **2016**, *138*, 14574−14577.

(11) Kieslich, G.; Birkel, C. S.; Stewart, A.; Kolb, U.; Tremel, W. Solution Synthesis of Nanoparticular Binary Transition Metal Antimonides. *Inorg. Chem.* **2011**, *50*, 6938−6943.

(12) Heise, M.; Chang, J.-H.; Schönemann, R.; Herrmannsdörfer, T.; Wosnitza, J.; Ruck, M. Full Access to Nanoscale Bismuth-Palladium Intermetallics by Low-Temperature Syntheses. *Chem. Mater.* **2014**, *26*, 5640−5646.

(13) Xie, J.; Zhao, X. B.; Yu, H. M.; Qi, H.; Cao, G. S.; Tu, J. P. Low Temperature Solvothermal Synthesis of Nanosized NiSb as a Li-ion Battery Anode Material. *J. Alloys Compd.* **2007**, *441*, 231−235.

(14) Teichert, J.; Heise, M.; Chang, J.-H.; Ruck, M. Refinement of the Microwave-Assisted Polyol Process for the Low-Temperature Synthesis of Intermetallic Nanoparticles. *Eur. J. Inorg. Chem.* **2017**, 4930−4938.

(15) Cable, R. E.; Schaak, R. E. Low-Temperature Solution Synthesis of Nanocrystalline Binary Intermetallic Compounds Using the Polyol Process. *Chem. Mater.* **2005**, *17*, 6835−6841.

(16) Chou, N. H.; Schaak, R. E. Shape-Controlled Conversion of β-Sn Nanocrystals into Intermetallic M-Sn (M = Fe, Co, Ni, Pd) Nanocrystals. *J. Am. Chem. Soc.* **2007**, *129*, 7339−7345.

DOI: 10.1021/acsomega.9b00088
ACS Omega 2019, 4, 5197−5203

(17) Henderson, N. L.; Schaak, R. E. Low Temperature Solution-Mediated Synthesis of Polycrystalline Intermetallic Compounds from Bulk Metal Powders. *Chem. Mater.* **2008**, *20*, 3212−3217.
(18) Henderson, N. L.; Straesser, M. D.; Sabato, P. E.; Schaak, R. E. Toward Green Metallurgy: Low-Temperature Solution Synthesis of Bulk-Scale Intermetallic Compounds in Edible Plant and Seed Oils. *Green Chem.* **2009**, *11*, 974−978.
(19) Da Silva, M. R.; Dias Ângelo, A. C. Synthesis and Characterization of Ordered Intermetallic Nanostructured PtSn/C and PtSb/C and Evaluation as Electrodes for Alcohol Oxidation. *Electrocatalysis* **2010**, *1*, 95−103.
(20) Maligal-Ganesh, R. V.; Xiao, C.; Goh, T. W.; Wang, L.-L.; Gustafson, J.; Pei, Y.; Qi, Z.; Johnson, D. D.; Zhang, S.; Tao, F. A Ship-in-a-Bottle Strategy to Synthesize Encapsulated Intermetallic Nanoparticle Catalysts: Exemplified for Furfural Hydrogenation. *ACS Catal.* **2016**, *6*, 1754−1763.
(21) Malik, M. A.; Afzaal, M.; O'Brien, P. Precursor Chemistry for Main Group Elements in Semiconducting Materials. *Chem. Rev.* **2010**, *110*, 4417−4446.
(22) McElwee-White, L. Design of Precursors for the CVD of Inorganic Thin Films. *Dalton Trans.* **2006**, 5327−5333.
(23) Cowley, A. H.; Jones, R. A. The Single-Source Precursor Concept. A Case Study of Gallium Arsenide. *Polyhedron* **1994**, *13*, 1149−1157.
(24) Winter, C. H. The Chemical Vapor Deposition of Metal Nitride Films Using Modern Metalorganic Precursors. *Aldrichimica Acta* **2000**, *33*, 3−8.
(25) Buhro, W. E. Progress in Molecular Precursors for Electronic Materials. *Adv. Mater. Opt. Electron.* **1996**, *6*, 175−184.
(26) Wooten, A. J.; Werder, D. J.; Williams, D. J.; Casson, J. L.; Hollingsworth, J. A. Solution-Liquid-Solid Growth of Ternary Cu-In-Se Semiconductor Nanowires from Multiple- and Single-Source Precursors. *J. Am. Chem. Soc.* **2009**, *131*, 16177−16188.
(27) Trindade, T.; O'Brien, P. Synthesis of CdS and CdSe Nanocrystallites Using a Novel Single-Molecule Precursors Approach. *Chem. Mater.* **1997**, *9*, 523−530.
(28) Dhanapala, B. D.; Munasinghe, H. N.; Suescun, L.; Rabuffetti, F. A. Bimetallic Trifluoroacetates as Single-Source Precursors for Alkali−Manganese Fluoroperovskites. *Inorg. Chem.* **2017**, *56*, 13311−13320.
(29) Buhro, W. E. Metallo-Organic Routes to Phosphide Semiconductors. *Polyhedron* **1994**, *13*, 1131−1148.
(30) Groom, C. R.; Bruno, I. J.; Lightfoot, M. P.; Ward, S. C. The Cambridge Structural Database. *Acta Crystallogr., Sect. B: Struct. Crystallogr. Cryst. Chem.* **2016**, *72*, 171−179.
(31) Jones, J. S.; Wade, C. R.; Yang, M.; Gabbaï, F. P. On the Coordination Non-Innocence of Antimony in Nickel(II) Complexes of the Tetradentate $(o\text{-}(Ph_2P)C_6H_4)_3Sb$ Ligand. *Dalton Trans.* **2017**, *46*, 5598−5604.
(32) Jones, J. S.; Wade, C. R.; Gabbaï, F. P. Redox and Anion Exchange Chemistry of a Stibine-Nickel Complex: Writing the L, X, Z Ligand Alphabet with a Single Element. *Angew. Chem., Int. Ed.* **2014**, *53*, 8876−8879.
(33) Ke, I.-S.; Gabbaï, F. P. σ-Donor/Acceptor-Confused Ligands: The Case of a Chlorostibine. *Inorg. Chem.* **2013**, *52*, 7145−7151.
(34) Jones, J. S.; Wade, C. R.; Gabbaï, F. P. Guilty on Two Counts: Stepwise Coordination of Two Fluoride Anions to the Antimony Atom of a Noninnocent Stibine Ligand. *Organometallics* **2015**, *34*, 2647−2654.
(35) Sahu, S.; Gabbaï, F. P. Photoreductive Elimination of Chlorine from Antimony in an $[SbPd]^{VII}$ Complex. *J. Am. Chem. Soc.* **2017**, *139*, 5035−5038.
(36) Villars, P.; Okamoto, H.; Cenzual, K. ASM Alloy Phase Diagrams Database. https://matdata.asminternational.org/apd/index.aspx (accessed July 11, 2018).
(37) Andaraarachchi, H. P.; Thompson, M. J.; White, M. A.; Fan, H.-J.; Vela, J. Phase-Programmed Nanofabrication: Effect of Organophosphite Precursor Reactivity on the Evolution of Nickel and Nickel Phosphide Nanocrystals. *Chem. Mater.* **2015**, *27*, 8021−8031.
(38) Guo, Y.; Alvarado, S. R.; Barclay, J. D.; Vela, J. Shape-Programmed Nanofabrication: Understanding the Reactivity of Dichalcogenide Precursors. *ACS Nano* **2013**, *7*, 3616−3626.
(39) Ruberu, T. P. A.; Albright, H. R.; Callis, B.; Ward, B.; Cisneros, J.; Fan, H.-J.; Vela, J. Molecular Control of the Nanoscale: Effect of Phosphine Chalcogenide Reactivity on CdS-CdSe Nanocrystal Composition and Morphology. *ACS Nano* **2012**, *6*, 5348−5359.
(40) Brutchey, R. L. Diorganyl Dichalcogenides as Useful Synthons for Colloidal Semiconductor Nanocrystals. *Acc. Chem. Res.* **2015**, *48*, 2918−2926.
(41) Hendricks, M. P.; Campos, M. P.; Cleveland, G. T.; Jen-La Plante, I.; Owen, J. S. A Tunable Library of Substituted Thiourea Precursors to Metal Sulfide Nanocrystals. *Science* **2015**, *348*, 1226−1230.
(42) Glassy, B. A.; Cossairt, B. M. II_3V_2 (II: Zn, Cd; V: P, As) Semiconductors: From Bulk Solids to Colloidal Nanocrystals. *Small* **2017**, *13*, 1702038.
(43) Rhodes, J.; Jones, C.; Thal, L.; Macdonald, J. E. Phase-Controlled Colloidal Syntheses of Iron Sulfide Nanocrystals via Sulfur Precursor Reactivity and Direct Pyrite Precipitation. *Chem. Mater.* **2017**, *29*, 8251−8530.
(44) Wang, Y.; Alsmeyer, D. C.; McCreery, R. L. Raman Spectroscopy of Carbon Materials: Structural Basis of Observed Spectra. *Chem. Mater.* **1990**, *2*, 557−563.
(45) Chu, P. K.; Li, L. Characterization of Amorphous and Nanocrystalline Carbon Films. *Mater. Chem. Phys.* **2006**, *96*, 253−277.
(46) Pimenta, M. A.; Dresselhaus, G.; Dresselhaus, M. S.; Cançado, L. G.; Jorio, A.; Saito, R. Studying Disorder in Graphite-Based Systems by Raman Spectroscopy. *Phys. Chem. Chem. Phys.* **2007**, *9*, 1276−1290.
(47) Lin, C.-C.; Guo, Y.; Vela, J. Microstructure Effects on the Water Oxidation Activity of Co_3O_4/Porous Silica Nanocomposites. *ACS Catal.* **2015**, *5*, 1037−1044.
(48) Qi, Z.; Pei, Y.; Goh, T. W.; Wang, Z.; Li, X.; Lowe, M.; Maligal-Ganesh, R. V.; Huang, W. Conversion of Confined Metal@ZIF-8 Structures to Intermetallic Nanoparticles Supported on Nitrogen-doped Carbon for Electrocatalysis. *Nano Res.* **2018**, *11*, 3469−3479.
(49) Mohapatra, P.; Shaw, S.; Mendivelso-Perez, D.; Bobbitt, J. M.; Silva, T. F.; Naab, F.; Yuan, B.; Tian, X.; Smith, E. A.; Cademartiri, L. Calcination Does Not Remove All Carbon from Colloidal Nanocrystal Assemblies. *Nat. Commun.* **2017**, *8*, 2038.
(50) Shaw, S.; Colaux, J. L.; Hay, J. L.; Peiris, F. C.; Cademartiri, L. Building Materials from Colloidal Nanocrystal Arrays: Evolution of Structure, Composition, and Mechanical Properties upon the Removal of Ligands by O_2 Plasma. *Adv. Mater.* **2016**, *28*, 8900−8905.
(51) Mohapatra, P.; Mendivelso-Perez, D.; Bobbitt, J. M.; Shaw, S.; Yuan, B.; Tian, X.; Smith, E. A.; Cademartiri, L. Large Scale Synthesis of Colloidal Si Nanocrystals and their Helium Plasma Processing into Spin-On, Carbon-Free Nanocrystalline Si Films. *ACS Appl. Mater. Interfaces* **2018**, *10*, 20740−20747.
(52) Shaw, S.; Tian, X.; Silva, T. F.; Bobbitt, J. M.; Naab, F.; Rodrigues, C. L.; Smith, E. A.; Cademartiri, L. Selective Removal of Ligands from Colloidal Nanocrystal Assemblies with Non-Oxidizing He Plasmas. *Chem. Mater.* **2018**, *30*, 5961−5967.
(53) Palazon, F.; Chen, F.; Akkerman, Q. A.; Imran, M.; Krahne, R.; Manna, L. Effects of Oxygen Plasma on the Chemical, Light-Emitting, and Electrical-Transport Properties of Inorganic and Hybrid Lead Bromide Perovskite Nanocrystal Films. *ACS Appl. Nano Mater.* **2018**, *1*, 5396−5400.
(54) Barbiéri, R. S.; Belatto, C. R.; Massabni, A. C. Thermal Analyses of Coordination Compounds II. Thermal Decomposition of Palladium Complexes with Triphenylphosphine, Triphenylarsine and Triphenylstibine. *J. Therm. Anal.* **1995**, *44*, 903−909.

DOI: 10.1021/acsomega.9b00088
ACS Omega 2019, 4, 5197−5203